Residual strain effects on a non-contact magnetoelastic torque transducer

R. Andreescu[a], B. Spellman[b,*] and E.P. Furlani[c]

[a]*Applied Research Center, 12000 Jefferson Avenue, Newport News, VA, USA*
[b]*Formerly with Continental, 100 Electronics Blvd, Huntsville, AL, USA*
Currently with BAE Systems, 308 Voyager Drive, Huntsville AL, USA
[c]*Eastman Kodak Company, 343 State Street, Rochester, NY, USA*

Abstract. A non-contact magnetoelastic torque transducer consisting of a non-magnetic shaft with a portion of its length coated with a magnetostrictive material is studied. A phenomenological theory is developed for predicting the magnetic field of the transducer as a function of coating properties, residual strain, and applied torque. This theory takes into account stress-induced anisotropy and variations in magnetoelastic energy within the coating. The resulting model is used to investigate the effect of quiescent stress states on the sensitivity, hysteresis and linearity.

Keywords: Magnetic torque sensor, non-contact torque sensor, magnetoelastic sensor, magnetostrictive torque sensor

1. Introduction

Magnetomechanical interactions are attracting considerable interest from both scientific groups and industry [1,2]. One of the numerous applications of this field of study is the ability to sense and measure torque on a member without physical contact. This is a primary objective in numerous automotive, industrial, and machining applications. A simple magnetostrictive ring sensor for this purpose has been proposed by Garshelis [3]. The operation of this sensor is based on a stress-induced rotation of magnetization within a magnetic coating that is rigidly attached to a non-magnetic torqued shaft (Fig. 1). The attached coating has a residual strain-induced easy axis of magnetization around its circumference, and is initially magnetized by passing a pulsed current through the shaft so that its magnetization is oriented along its circumference, in alignment with the residual magnetoelastic anisotropy. The magnetoelastic anisotropy within the ring is altered when the shaft has torque applied; consequently, the magnetization vector rotates away from the circumferential direction towards the newly formed easy axis created by the applied torque. An axial polarization develops due to the rotated magnetization creating surface poles at both of its ends and leading to a magnetic field outside the coating. Thus, an applied torque produces a measurable magnetic field which can be detected by a magnetometer in proximity to the coating. In this way, the torque can be sensed and measured without any contact between the shaft and the measuring instrument.

There are many applications for non-contact torque sensors as such sensors enable torque measurements of spinning shafts without the cumbersome use of slip rings or expense of RF links. The sensor described

---

*Corresponding author. Tel.: +1 256 864 7039; E-mail: bert.spellman@knology.net.
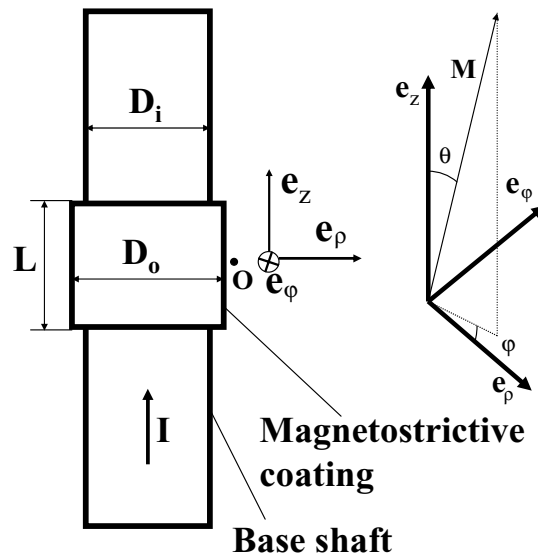
Fig. 1. Non-contact magnetoelastic torque transducer.

in this paper can measure the torque input of the driver on a steering shaft of an automobile. Accurate measurements of this value enable the application of power assist which limits the effort required by the driver to steer the vehicle. Furthermore, a steering system must withstand severe over torques without altering the torque signal, therefore, an emphasis is placed on hysteretic effects. The sensor described below can also be used to measure the torque on transmission shafts in-situ, thereby allowing for shift point control regardless of ambient conditions resulting in the shift feel of the transmission remaining constant over the life of the transmission. Torque transfer of all-wheel-drive vehicles can also benefit from this sensor as the torque can be accurately applied to the front or rear axles to improve drivability of the vehicle. In addition, the measurement of individual wheel torque will be most useful and beneficial in future torque vectoring applications wherein the torque applied to each driven wheel can be controlled to improve drivability and stability of vehicular systems.

A phenomenological theory developed for predicting the performance of such a magnetostrictive transducer was described in [4]. In that article it was shown how various levels of residual strain influence transducer behavior. In the present work two parameters (Sensitivity and Hysteresis) are introduced and it is shown how the overall performance of the sensor can be optimized.

2. Theory

The phenomenological model presented here and in [4] is independent of microscopic mechanisms. Specifically, defect-free single crystals are considered whose behavior is governed by energy terms that are independent of the microscopic arrangement. These energy terms include the magnetocrystalline energy, the magnetoelastic energy, the magnetostatic energy (magnetostatic effects are treated independently of the internal structure by using demagnetizing constants, which give rise to a correspondingly uniform demagnetizing field), and the energy of interaction with the applied field.

Consider for the moment the magnetocrystalline anisotropy term u_{anis} and the magnetoelastic term

u_{me}. The magnetic free energy of a cubic material is (ref. [3]):

$$
\begin{aligned}
u &= u_{anis} + u_{me} \\
&= K_1(\alpha_1^2\alpha_2^2 + \alpha_2^2\alpha_3^2 + \alpha_3^2\alpha_1^2) + K_2\alpha_1^2\alpha_2^2\alpha_3^2 + \ldots \\
&\quad + B_1\left[e_{xx}\left(\alpha_1^2 - \frac{1}{3}\right) + e_{yy}\left(\alpha_2^2 - \frac{1}{3}\right) + e_{zz}\left(\alpha_3^2 - \frac{1}{3}\right)\right] \\
&\quad + B_2(e_{xy}\alpha_1\alpha_2 + e_{yz}\alpha_2\alpha_3 + e_{zx}\alpha_3\alpha_1) + \ldots
\end{aligned}
\tag{1}
$$

where K_1 and K_2 are magnetic anisotropy constants, B_1 and B_2 are magnetoelastic coefficients, α_1, α_2 and α_3 are the direction cosines of the magnetization along the three coordinate axes, and e_{ij} are the strain components.

A single-crystal with cubic symmetry is placed on a shaft with its lattice parallel to the cylindrical unit vectors $\mathbf{e}_\rho$, $\mathbf{e}_\varphi$, $\mathbf{e}_z$ as shown in Fig. 1. Replacing α_1, α_2 and α_3 with γ_1, γ_2 and γ_3 (the direction cosines of the magnetization along $\mathbf{e}_\rho$, $\mathbf{e}_\varphi$, $\mathbf{e}_z$, respectively) and the strain components with the strain components relative to the cylindrical coordinate system Eq. (1) is transformed into an equation describing this embodiment. Adding the magnetostatic energy and the energy of interaction with the external field, the magnetic free energy of the cubic lattice on a cylindrical substrate becomes:

$$
\begin{aligned}
u &= u_{anis} + u_{me} + u_d + u_a \\
&= K_1(\gamma_1^2\gamma_2^2 + \gamma_2^2\gamma_3^2 + \gamma_3^2\gamma_1^2) + K_2\gamma_1^2\gamma_2^2\gamma_3^2 + \ldots \\
&\quad + B_1\left[e_{\rho\rho}\left(\gamma_1^2 - \frac{1}{3}\right) + e_{\phi\phi}\left(\gamma_2^2 - \frac{1}{3}\right) + e_{zz}\left(\gamma_3^2 - \frac{1}{3}\right)\right] + B_2(e_{\rho\phi}\gamma_1\gamma_2 + e_{\phi z}\gamma_2\gamma_3 \\
&\quad + e_{z\rho}\gamma_3\gamma_1) + \ldots + \frac{1}{2}\mu_0 M_S^2(N_{dz}\gamma_3^2 + N_{d\rho}\gamma_3^2) - \mu_0 M_S H_a\gamma_2
\end{aligned}
\tag{2}
$$

where N_{dz} and $N_{d\rho}$ are demagnetizing factors, H_a is the applied field, and M_s is the spontaneous magnetization. H_a is created by a pulsed current as shown in Fig. 1 which is designed to saturate the coating in the tangential direction. After removal of H_a, the coating remains in magnetized state and torques may be applied.

The strains in Eq. (2) are experimentally set as follows: The tangential strain $e_{\Phi\Phi} = e_{\Phi\Phi}^0$ is induced in the coating through a thermal treatment and this strain creates an easy axis of magnetization in the tangential direction. The thermal treatment also induces axial and radial strains $e_{zz} = e_{zz}^0$ and $e_{\rho\rho} = e_{\rho\rho}^0$ which will be considered in the following. Shear strains $e_{\rho\Phi}$ and $e_{z\rho}$, induced in the coating by the thermal treatment, are small and therefore can be neglected. In addition, any applied torque τ will induce a shear strain $e_{\Phi z}$ and this strain depends on the torque as well as the shaft and coating properties, i.e.

$$
e_{\phi z} = \frac{r}{G_C J_C + G_S J_S}\tau
\tag{3}
$$

This value is valid in the coating with r between $D_i/2$ and $D_O/2$ (see Fig. 1). G_C is the torsional modulus of elasticity in the coating and G_S is the torsional modulus of elasticity for the shaft. The coating's moment of inertia is $J_C = \frac{\pi}{32}(D_O^4 - D_i^4)$ and the shaft's is $J_S = \frac{\pi}{32}(D_{OS}^4 - D_{iS}^4)$ where $D_{OS} = D_i$ and D_{iS} are the outer and inner diameters of the shaft (D_{iS} is not shown in Fig. 1).

Rotating the lattice cube edges parallel to $\mathbf{e}_\rho$, $\mathbf{e}_\varphi$ and $\mathbf{e}_z$ in three steps: first by an angle g1 about $\mathbf{e}_\rho$, then by an angle g_2 about $\mathbf{e}_\varphi$, and finally by an angle g_3 about $\mathbf{e}_z$, the matrix describing this rotation is:

$$R = \begin{bmatrix} 1 & 0 & 0 \\ 0 & \cos(g_1) & -\sin(g_1) \\ 0 & \sin(g_1) & \cos(g_1) \end{bmatrix} \begin{bmatrix} \cos(g_2) & 0 & \sin(g_2) \\ 0 & 1 & 0 \\ -\sin(g_2) & 0 & \cos(g_2) \end{bmatrix} \begin{bmatrix} \cos(g_3) & -\sin(g_3) & 0 \\ \sin(g_3) & \cos(g_3) & 0 \\ 0 & 0 & 1 \end{bmatrix} \tag{4}$$

The new direction cosines of the magnetization with respect to the cube edges of the rotated lattice are γ_1', γ_2', and γ_3' are given by:

$$[\gamma_1' \gamma_2' \gamma_3']^T = R[\gamma_1 \gamma_2 \gamma_3]^T \tag{5}$$

where $[\ ]^T$ denotes the transposed matrix.

The strains with respect to the rotated lattice are:

$$\begin{bmatrix} e_{11}' & e_{12}' & e_{13}' \\ e_{21}' & e_{22}' & e_{23}' \\ e_{31}' & e_{32}' & e_{33}' \end{bmatrix} = R \begin{bmatrix} e_{\rho\rho}^0 & 0 & 0 \\ 0 & e_{\phi\phi}^0 & e_{\phi z}(\tau) \\ 0 & e_{\phi z}(\tau) & e_{zz}^0 \end{bmatrix} R^T \tag{6}$$

The free energy of the cubic lattice rotated by g_1, g_2, g_3 about $\mathbf{e}_\rho$, $\mathbf{e}_\varphi$, $\mathbf{e}_z$ is:

$$\begin{aligned} u &= u_{anis} + u_{me} + u_d + u_a \\ &= K_1(\gamma_1'^2 \gamma_2'^2 + \gamma_2'^2 \gamma_3'^2 + \gamma_3'^2 \gamma_1'^2) + K_2 \gamma_1'^2 \gamma_2'^2 \gamma_3'^2 + \ldots \\ &\quad + B_1 \left[e_{11}'\left(\gamma_1'^2 - \frac{1}{3}\right) + e_{22}'\left(\gamma_2'^2 - \frac{1}{3}\right) + e_{33}'\left(\gamma_3'^2 - \frac{1}{3}\right) \right] + \ldots \\ &\quad + B_2(\gamma_1'^2 \gamma_2'^2 e_{12}' + \gamma_2'^2 \gamma_3'^2 e_{23}' + \gamma_3'^2 \gamma_1'^2 e_{31}') + \ldots \\ &\quad + \frac{1}{2}\mu_0 M_S^2 (N_{dz}\gamma_3^2 + N_{d\rho}\gamma_1^2) - \mu_0 M_S H_a \gamma_2 \end{aligned} \tag{7}$$

Magnetization orientation expressed with respect to $\mathbf{e}_\rho$, $\mathbf{e}_\varphi$, $\mathbf{e}_z$ requires angles θ and φ to be defined (see Fig. 1) as:

$$\gamma_1 = \sin(\theta)\cos(\varphi), \gamma_2 = \sin(\theta)\sin(\phi), \gamma_3 = \cos(\theta) \tag{8}$$

The γ_i in Eq. (8) are substituted into Eq. (5) to obtain γ_i'. Utilizing γ_i' and e_{ij}', as specified in Eq. (6), in Eq. (7) the functional form of the free energy becomes:

$$u = u(\theta, \phi, g_1, g_2, g_3, e_{\phi\phi}^0, e_{zz}^0, e_{\rho\rho}^0, \tau, H_a) \tag{9}$$

The free energy can now be minimized with respect to θ and Φ utilizing g_1, g_2, g_3, $e_{\Phi\Phi}^0$, e_{zz}^0, $e_{\rho\rho}^0$, τ, H_a as parameters to obtain the orientation of magnetization.

For practical steering torque applications, the range of -8 N·m to 8 N·m needs to be accurately measured. The transducer must also be capable of withstanding transient high torques (up to hundreds of N·m) acting on the system. The transducer must be designed so these high torques do not degrade its performance over its nominal operating range. Thus, before studying the transducer in its normal operating range, high torque is applied to the shaft in the laboratory.

To model the behavior of the system the parameters g_1, g_2, g_3, $e_{\Phi\Phi}^0$, e_{zz}^0, $e_{\rho\rho}^0$ are initially fixed. One starts with an unambiguous initial state (i.e., the state with $\theta = 90^0$, $\varphi = 90^0$ in which the free energy

has a unique minimum), corresponding to a large applied field H_a which saturates the system. H_a is progressively reduced to zero keeping $\tau = 0$. Next, keeping $H_a = 0$, τ is varied and the dependence of φ (τ) and $\theta(\tau)$ is traced (minimizing u with respect to θ and φ) for a cycle of τ between -400 and 400 N·m, followed by a cycle of τ between -8 and 8 N·m. During these steps, while H_a and then τ are varying, the free energy u has, in general, a complicated profile, with both minima (which in some circumstances can be occupied by the system) and maxima. Moreover, this energy profile changes continuously during the variation of H_a and τ. Generally in this process the evolution of the system is not a succession of equilibrium states (that is, the orientation of the magnetization for a certain applied field or torque is not always given by the absolute minimum of the free energy); actually for many field and torque values, the system is trapped in local minima (metastable states) which it cannot leave to occupy the state of absolute minimum – in these situations the system presents hysteresis.

The orientation of the magnetization is defined by φ (τ) and $\theta(\tau)$ obtained in the above process as the torque is varied. The external magnetic field of the transducer created at an observation point O (see Fig. 1) is calculated using the magnetic "charge" model in which

$$B(r) = \frac{\mu_0}{4\pi} \int_V \frac{\rho_m(r - r')}{|r - r'|^3} dV' + \frac{\mu_0}{4\pi} \int_\Sigma \frac{\sigma_m(r - r')}{|r - r'|^3} da' \tag{10}$$

where $\rho_m = -\nabla \cdot M$ and $\sigma_m = M \cdot \hat{n}$ are the volume and surface charge densities, respectively, and $\hat{n}$ is the unit vector normal to the surface (see in [6, pp. 131–135]). The surface integral is evaluated over the coating surface Σ, and the volume integral is evaluated over the coating volume V.

3. Results

Applying the theory to a transducer where the magnetic coating is taken to be crystalline Ni with the following dimensions: $D_i = 28.5$ mm, $D_O = 29.5$ mm, and $L = 44.7$ mm and with parameters as supplied in refs. [5,7] as: $K_1 = -4500$ J/m^3, $K_2 = -2300$ J/m^3, $B_1 = 6.2 \cdot 10^6$ N/m^2, $B_2 = 4.3 \cdot 10^6$ N/m^2, $M_s = 450000$ A/m, $N_{dz} = 0.012$ and $N_{d\rho} = 0.98$. The base shaft is a non-magnetic stainless steel of inner and outer diameters: $D_{iS} = 15.86$ mm, $D_{OS} = D_i$. The moduli of elasticity in torsion for the base shaft and the coating are $G_s = 76.5$ GPa and $G_{Ni} = 76$ GPa. The coating is modeled as a single layer at the mid-point resulting in $e_{\Phi z}$ given by (3) for r half way between $D_i/2$ and $D_O/2$ as $e_{\Phi z}(\tau) = 2.66 \cdot 10^{-6}\tau$; this function for shear strain in the coating will be substituted into (2) and used in the following calculations.

Substituting the numerical values into Eq. (9) and stepping through the reduction of free energy and application of torque as described earlier, the energy minima can be determined resulting in the magnetization orientation as a function of applied torque being determined. This can be done for various initial strain states $\{e_{\Phi\Phi}^0, e_{zz}^0, e_{\rho\rho}^0\}$ and crystal lattice orientations $\{g1, g2, g3\}$. The external axial magnetic field versus torque, B_{axial} vs. τ, can then be obtained via Eq. (10).

Next, to estimate the average values of θ and φ in a coating of weakly-interacting, randomly-oriented crystallites during the application of the torque, it is assumed that the system can be approximated by the superposition of contributions from many single-crystal lattices (like the ones discussed so far) randomly oriented in space. Consequently, the dependencies of $\theta(\tau)$ and $\varphi(\tau)$, then $B_{axial}(\theta(\tau),\varphi(\tau))$, are calculated for a number of 1000 orientations $\{g_i, g_j, g_k\}_{i,j,k=1,...,10}$ drawn with a uniform distribution by the computer. Then an average taken over the 1000 orientations is performed and $B_{axial}(\tau)$ is traced.
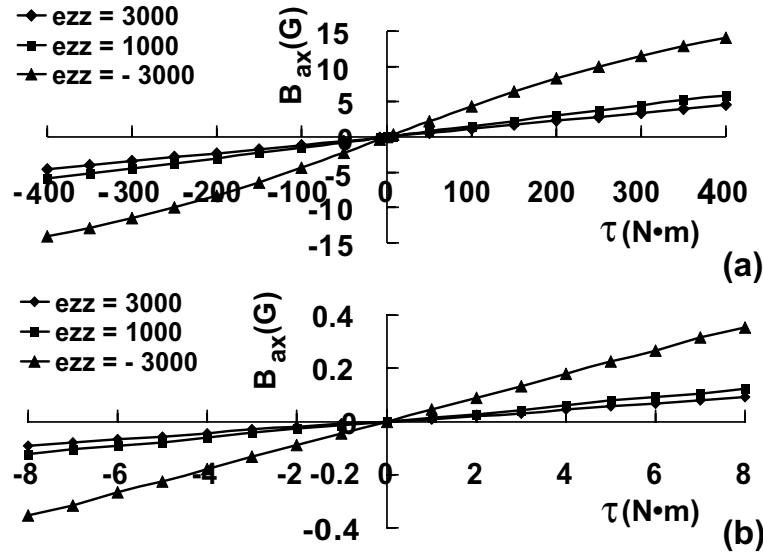
Fig. 2. Axial magnetic field created by the Ni coating under residual axial strains $e_{zz}^0 = -3000$ μstrain, 1000 μstrain, 3000 μstrain. The tangential residual strain is $e_{\varphi\varphi}^0 = -5000$ μstrain, the radial residual strain is $e_{\rho\rho}^0 = 0$ μstrain. The magnetic field is measured in the middle, at a point situated at 0.25 mm from the coating.

Figures 2–6 show curves B_{axial} vs. τ for various residual strains. The axial component B_{axial} is measured at a point O (shown in Fig. 1) situated in the middle, at a distance of 0.25 mm from the coating.

In Fig. 2 it is shown, for a maximum applied torque of 400 N·m (a) and for a maximum applied torque of 8 N·m (b), how the residual axial strain influences the transducer behavior (the tangential and radial residual strain are fixed to $e_{\Phi\Phi}^0 = -5000$ μstrain and $e_{\rho\rho}^0 = 0$ μstrain). For $e_{zz}^0 = 3000$ μstrain, the average slope of the curve $B_{\text{axial}} - \tau$ is small. The axial direction is a strong hard axis (created by the tensile residual strain) which pushes the magnetization towards the easy axis (tangential direction). In this case, the applied torque barely rotates the magnetization away from the tangential direction. Decreasing the tensile axial strain to $e_{zz}^0 = 1000$ μstrain will weaken the axial hard axis and the applied torque will rotate the magnetization more easily resulting in the average slope of the curve $B_{\text{axial}} - \tau$ increasing. If the axial strain is compressive ($e_{zz}^0 = -3000$ μstrain) the axial direction becomes an easy axis, which helps the applied torque to rotate the magnetization away from the tangential direction. Consequently, for $e_{zz}^0 = -3000$ μstrain the average slope of the curve $B_{\text{axial}} - \tau$ is larger than in the previous cases.

For the values of the axial strain shown in Fig. 2 the free energy has one minimum for $\tau = 0$; this sole state is attained by the system through both positive and negative applications of torque. In consequence, the system shows no hysteresis. For axial larger compressive strains the system does show hysteresis. Examples of curves $B_{\text{axial}} - \tau$ with hysteresis are shown in Figs 3, 4 and 5.

In Fig. 3, maximum applied torques of 400 N·m and 8 N·m are applied to systems with residual strains of $e_{\Phi\Phi}^0 = 5000$ μstrain, $e_{\rho\rho}^0 = 0$ μstrain, $e_{zz}^0 = -3260$ μstrain in the coating. With these initial conditions, the system shows hysteresis. The reason is that the axial easy axis (together with the tangential easy axis and the crystalline anisotropy) creates for $\tau = 0$ two minima which the system occupies in turns (one when the system attains state $\tau = 0$ through positive values, the other one when the system attains state $\tau = 0$ through negative values).

Figure 4 is similar to Fig. 3 the only difference being a larger axial residual strain, $e_{zz}^0 = -3276$ μstrain. Comparison between Figs 3 and 4 show that both curves $B_{\text{axial}} - \tau$ have hysteresis and the average slope
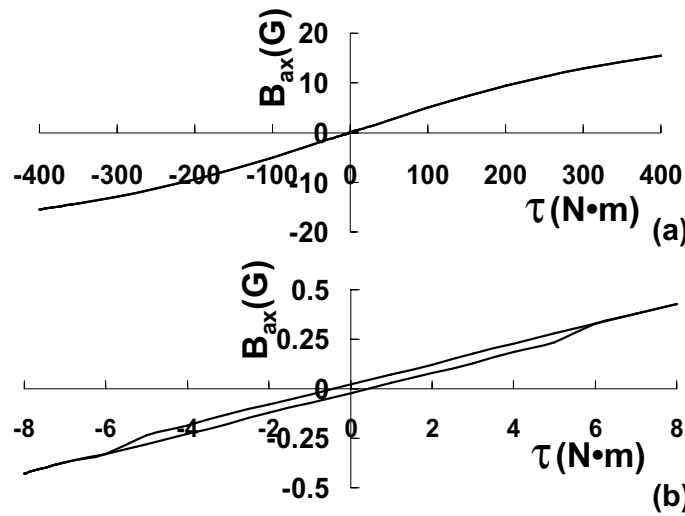
Fig. 3. Hysteresis loops B_{axial} vs. applied torque for a Ni coating under residual strains $e^0_{\varphi\varphi} = -5000\ \mu$strain, $e^0_{\rho\rho} = 0\ \mu$strain, $e^0_{zz} = -3260\ \mu$strain. The magnetic field is measured in the middle, at a point situated at 0.25 mm from the coating. (a) Maximum applied torque 400 N·m (b) Maximum applied torque 8 N·m.
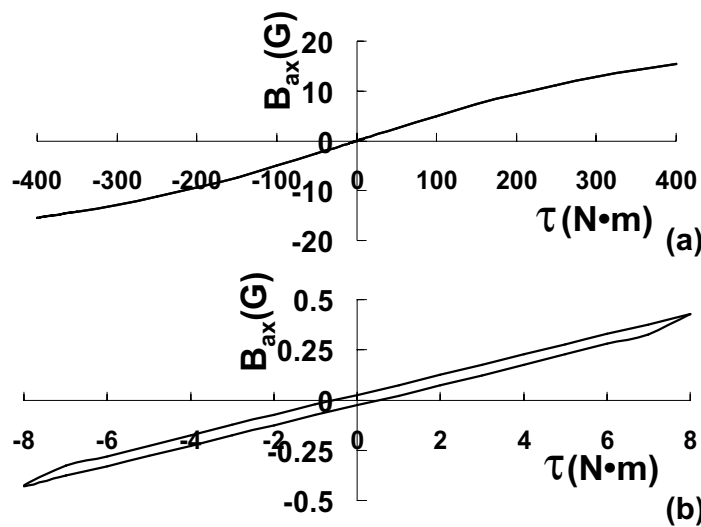
Fig. 4. Hysteresis loops B_{axial} vs. applied torque for a Ni coating under residual strains $e^0_{\varphi\varphi} = -5000\ \mu$strain, $e^0_{\rho\rho} = 0\ \mu$strain, $e^0_{zz} = -3276\ \mu$strain. The magnetic field is measured in the middle, at a point situated at 0.25 mm from the coating. (a) Maximum applied torque 400 N·m (b) Maximum applied torque 8 N·m.

of the curve $B_{axial} - \tau$ increases with increasing the axial residual strain. The influence on transducer performance by initial strain states will be discussed in the next paragraphs.

Figure 5 shows, for a maximum applied torque of 400 N·m, the curve $B_{axial} - \tau$ for a coating under the residual strain, $e^0_{\Phi\Phi} = -5000\ \mu$strain, $e^0_{\rho\rho} = 0\ \mu$strain and $e^0_{zz} = -3500\ \mu$strain. To make hysteresis more evident, in Fig. 5(b) the curve is shown again with the abscissa between -30 N·m and 30 N·m. As expected, the average slope of the curve $B_{axial} - \tau$ is bigger than in Fig. 4, since the residual axial strain is larger than in Fig. 4.
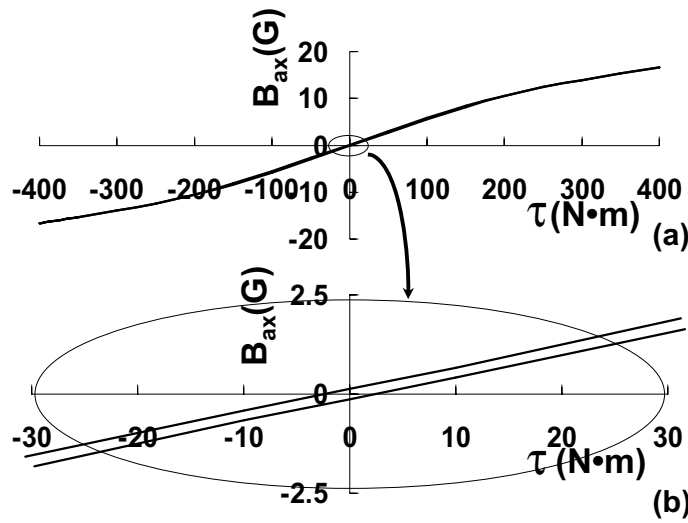
Fig. 5. Axial magnetic field created by the Ni coating under residual strain is $e^0_{\varphi\varphi} = -5000$ μstrain, $e^0_{\rho\rho} = 0$ μstrain, $e^0_{zz} = -3500$ μstrain. The magnetic field is measured in the middle, at a point situated at 0.25 mm from the coating. (a) Maximum applied torque 400 N·m. (b) Same as (a); to make hysteresis more evident, the loop in Fig. 5(a) is shown again with the abscissa between -30 and 30 N·m.
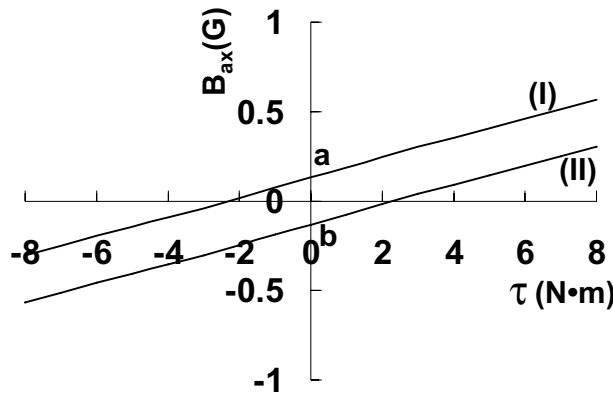

Fig. 6. Axial magnetic field created by the Ni coating under residual strain is $e^0_{\varphi\varphi} = -5000$ μstrain, $e^0_{\rho\rho} = 0$ μstrain, $e^0_{zz} = -3500$ μstrain for a maximum applied torque 8 N·m. The magnetic field is measured in the middle, at a point situated at 0.25 mm from the coating.

In Fig. 6 it is shown the curve $B_{axial} - \tau$ for the same residual strain as in Fig. 5, but with a maximum applied torque of 8 N·m. (as always in this article, a curve with a maximum applied torque of 8 N·m is preceded by the application of a +400-N·m or a - 400-N·m torque). It was seen in Fig. 5 that for a maximum applied torque of 400 N·m the system under residual strain $e^0_{\Phi\Phi} = -5000$ μstrain, $e^0_{\rho\rho} = 0$ μstrain and $e^0_{zz} = -3500$ μstrain shows hysteresis; however, from Fig. 6 it can be seen that the system under the same residual strain shows no hysteresis if the maximum applied torque is 8 N·m; moreover, it appears that for maximum applied torque of 8 N·m the system can follow one of the two lines shown in Fig. 6. A careful review of Figs 5 and 6 helps to explain this situation: After a hysteresis loop with a maximum applied torque of 400 N·m, the system is left in one of the states corresponding to $\tau = 0$ in
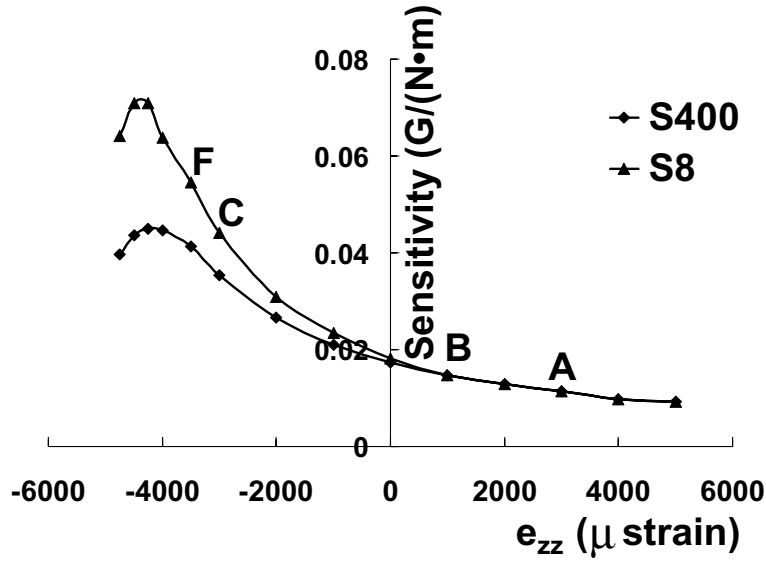
Fig. 7. Sensitivities S_{400} and S_8, as functions of the axial residual strain. The residual radial strain is $e_{\rho\rho}^0 = 0$ μstrain, the residual tangential strain is $e_{\varphi\varphi}^0 = -5000$ μstrain. The magnetic field is measured in the middle, at a point situated at 0.25 mm from the coating.

Fig. 5 (either in the state of positive remanence "a" or in the state of negative remanence "b") depending on the sign of the last applied maximum torque of 400 N·m. Now, starting from one of these states, torques between -8 and 8 N·m are applied. If the system starts from state "a", torques between -8 and 8 N·m will drive the system along the upper branch of the loop in Fig. 5 (that is, curve (I) in Fig. 6); if the system starts from state "b", torques between -8 and 8 N·m will take the system along the lower branch of the loop in Fig. 5 (that is, curve (II) in Fig. 6).

4. Transducer performance and optimization

In this section, two parameters describing transducer performance are studied: Sensitivity and Hysteresis. The Sensitivity of the transducer is defined as the slope of the line joining the extreme points of the graph B_{axial} vs. τ:

$$S_{\tau_0} = \frac{(B(\tau_0) - B(-\tau_0))}{2\tau_0} \tag{11}$$

where τ_0 is the absolute value of the maximum applied torque. Here τ_0 is either 400 N·m or 8 N·m.

The Hysteresis of the transducer can be defined as:

$$H_{\tau_0} = \frac{(B_{r+} - B_{r-})}{S_{\tau_0}} \tag{12}$$

where B_{r+} and B_{r-} are respectively the positive and negative remanence values on the hysteresis loop when the torque is varied between $-\tau_0$ and τ_0.

Figures 7 and 8 show calculated S_{400}, S_8, H_{400}, H_8, for several residual strains. The residual strains chosen to demonstrate transducer performance and optimization are $e_{\Phi\Phi}^0 = -5000$ μstrain, $e_{\rho\rho}^0 = 0$ μstrain, and e_{zz}^0 varying between 5000 and -4750 μstrain.
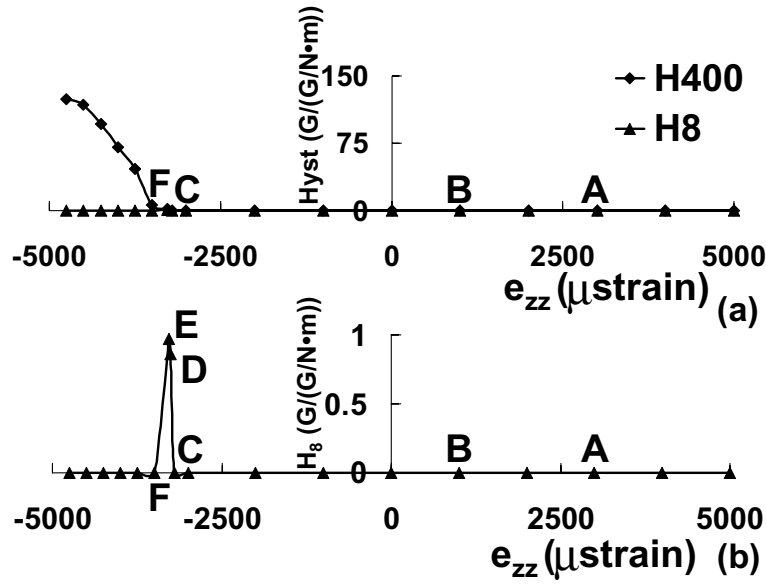
Fig. 8. Hysteresis as a function of the axial residual strain. The residual radial strain is $e^0_{\rho\rho} = 0$ μstrain, the residual tangential strain is $e^0_{\varphi\varphi} = -5000$ μstrain. (a) H_{400} and H_8. (b) H_8 is traced again; a different scale is used.

4.1. Sensitivity (Fig. 7)

In the right region of Fig. 7 (tensile axial strains) the axial direction is a strong hard axis which strengthens the tangential easy axis. In consequence the applied torque hardly rotates the magnetization and sensitivities S_{400} and S_8 will be very small. An example of such situation is point A, corresponding to the curve shown in Fig. 2 for $e^0_{zz} = 3000$ μstrain. Also, from Fig. 7 it can be seen that at point A the two sensitivities are equal $S_{400} = S_8$ (curve $B_{\text{axial}} - \tau$ is a straight line not only for torques between 0 and 8 N·m, but for torques between 0 and 400 N·m as well).

In Fig. 7, decreasing the tensile axial strain will cause the axial hard axis to weaken, the applied torque will rotate the magnetization more easily, and the sensitivity will increase. This situation is described by point B, which corresponds to the curve for $e^0_{zz} = 1000$ in Fig. 2. For point B the two sensitivities are again equal, ($S_{400} = S_8$), so curve $B_{\text{axial}} - \tau$ is again a straight line for torques between 0 and 8 N·m and for torques between 0 and 400 N·m.

Also in Fig. 7 for compressive (negative) axial strains from $e^0_{zz} = 0$ to about $e^0_{zz} = -4250$ μstrain, the axial direction becomes a stronger easy axis, which helps the applied torque to rotate the magnetization away from the tangential direction. Consequently, S_{400} and S_8 increase with increasing the magnitude of the compressive axial strain. Point C in Fig. 7 corresponds to the curve for $e^0_{zz} = -3000$ μstrain in Fig. 2 and point F in Fig. 7 corresponds to the curve in Fig. 5 at $e^0_{zz} = -3500$ μstrain respectively. From Fig. 7, it can be seen that for negative axial strains, $S_{400} < S_8$. This is an important characteristic; unlike the region of positive axial strains where $S_{400} = S_8$, the region of negative axial strains $B_{\text{axial}} - \tau$ curves for maximum applied torques of 400 Nm are S-shaped.

Examples of S-shaped curves can be seen in Fig. 2 for $e^0_{zz} = -3000$ μstrain and Fig. 5a. For increasing compressive strains from $e^0_{zz} = -4250$ μstrain to $e^0_{zz} = -4750$ μstrain, both sensitivities decrease. In this case, the axial easy axis is so strong that in the state of zero torque the magnetization vector is already displaced from the tangential direction. Starting from this situation, the application of the torque will

further rotate the magnetization, but not too much with respect to the state with $\tau = 0$. This will result in a decrease in sensitivity with increasing the magnitude of the axial compressive (negative) strain.

4.2. Hysteresis (*Fig. 8*)

It can be seen in Fig. 8 that for any value of the axial strain between 5000 and -3200 μstrain the system shows no hysteresis ($H_{400} = H_8 = 0$). In these cases the free energy has one minimum for $\tau = 0$ and this state is attained by the system through both positive and negative values of applied torque. Examples are points A, B and C, which correspond respectively to $B_{axial} - \tau$ curves in Fig. 2 for $e_{zz}^0 = 3000$ μstrain, 1000 μstrain and -3000 μstrain values of applied torque.

Also in Fig. 8, it appears that for compressive (negative) axial strains larger than 3200 μstrain in magnitude the system shows hysteresis; the axial easy axis (together with the tangential easy axis and the crystalline anisotropy) creates for $\tau = 0$ two minima which the system occupies in turn (one when the system attains state $\tau = 0$ through positive values, the other one when the system attains state $\tau = 0$ through negative values). For a maximum applied torque of 400 N·m, hysteresis increases with increasing the axial compressive strain (curve H400 in Fig. 8a). While for a maximum applied torque of 8 N·m, the situation is quite different: hysteresis increases with increasing axial compressive strain in a very narrow region (for ezz between -3200 and -3276 μstrain; examples are points D for $e_{zz} = -3260$ μstrain corresponding to Fig. 3, and E for $e_{zz} = -3276$ μstrain corresponding to Fig. 4) then hysteresis drops to zero at $e_{zz}^0 = -3276$ μstrain. This behavior was explained in the previous section.

From Figs 7 and 8, a maximum applied torque of 400 N·m yields the best sensitivity at approx. 0.045 G/N·m, corresponding to an axial residual stress of about -4250 μstrain and it is accompanied by hysteresis. The best sensitivity without hysteresis is approx. 0.04 G/N·m, and it is obtained for a compressive strain of about -3200 μstrain. For a maximum applied torque of 8 N·m, the maximum sensitivity is approx. 0.07 G/N·m, and is attained without hysteresis at about the same residual axial strain as the maximum sensitivity at 400 N·m.

5. Conclusions

The performance of a non-contact magnetoelastic-based torque transducer which consists of a magnetic coating attached to a non-magnetic shaft has been described via the minimization of the free energy of the system. An analysis of a prototype transducer is presented that demonstrates the use of the theory in identifying an optimal residual strain that maximizes transducer sensitivity at zero hysteresis. The theory developed herein is readily implemented and enables rapid parametric analysis of transducer performance.

References

[1] G.A. Maugin, *Continuum Mechanics of Electromagnetic Solids*, North-Holland, Amsterdam, Chapter X, 1988.
[2] E. Du Tremolet de Lacheisserie, *Magnetostriction: Theory and Application of Magnetoelasticity*, CRC, Boca Raton, Florida 1993.
[3] I.J. Garselis and C.R. Conto, *J Appl Phys* **79** (1996), 4756.
[4] R. Andreescu, B. Spellman and E.P. Furlani, *Journal of Magnetism and Magnetic Materials* **320** (2008), 1827–1833.
[5] R. O'Handley, Modern Magnetic Materials, 2000.
[6] E.P. Furlani, *Permanent Magnetic and Electromechanical Devices: Materials*, Analysis and Applications, Academic Press, New York, 2001.
[7] Hitachi Magnetics Corporation Guide circa, 1985.